

Nonuniform-spaced Critical Behavior of Dynamical Quantum Phase Transitions in Multi-band Bloch Hamiltonian

Kaiyuan Cao

Research Center for Intelligent Supercomputing, Zhejiang Laboratory, Hangzhou 311100, P. R. China

Hao Guo*

School of Physics, Southeast University, Jiaolonghu Campus, Nanjing 211189, P. R. China

Guangwen Yang[†]

Research Center for Intelligent Supercomputing, Zhejiang Laboratory, Hangzhou 311100, P. R. China and

*Department of Computer Science and Technology,
Tsinghua University, Beijing, Haidian, P. R. China*

(Dated: March 29, 2023)

We investigate the dynamical quantum phase transition (DQPT) in the multi-band Bloch Hamiltonian of the one-dimensional periodic Kitaev model after a quench from a Bloch band. Our study goes beyond the limitations of previous works that primarily focused on two-band models and reveals significant differences in DQPT between the two-band and multi-band systems. Our results show that only the quench from the Bloch states, which causes the band gap to collapse at the critical point, induces the DQPT after crossing the quantum phase transition; otherwise, the DQPT will not occur. Additionally, the critical times of the DQPT are not evenly spaced due to the deviation in the critical momentum caused by the non-analytic singularities of the Pancharatnam geometric phase. Our findings provide a better understanding of the characteristics of non-equilibrium systems surrounding DQPTs.

I. INTRODUCTION

Recent advancements in the experimental studies of ultra-cold atoms trapped in optical lattices^{1–3} provided a new framework for studying the non-equilibrium dynamics of isolated quantum systems⁴. In particular, the time evolution of a quantum system after a sudden global quench plays a crucial role in this field since it can be routinely carried out in experiments and studied in theoretical calculations⁵. When a quench occurs due to a sudden change in the parameter on which the Hamiltonian depends, the evolution is determined by the Loschmidt echo⁶, which is associated with the overlaps between the eigenstates of the pre-quench and post-quench Hamiltonians. Due to the formal analogy between the Loschmidt amplitude and the canonical partition function of an equilibrium system, the concept of dynamical quantum phase transition (DQPT) has been proposed to help understand the notions of phase and phase transition far from equilibrium, which has attracted significant interest in both the theoretical^{7–39} and experimental^{40–47} perspectives.

The DQPT describes non-analytic behaviors of the Loschmidt echo $\mathcal{L}(t) = |\mathcal{G}(t)|^2$ during the nonequilibrium dynamical evolution^{48–50}. The Loschmidt amplitude $\mathcal{G}(t)$ measures the overlap of the time-evolving state $|\psi(t)\rangle$ with its initial state $|\psi_0\rangle$, i.e.,

$$\mathcal{G}(t) = \langle \psi_0 | \psi(t) \rangle = \langle \psi_0 | e^{-iHt} | \psi_0 \rangle. \quad (1)$$

Here H refers to the final Hamiltonian of the system, which is reached through a sudden quench of parameters. Similar to equilibrium phase transitions, the DQPTs can

be identified by the cusp-like singularity of the rate function $\lambda(t) = -\lim_{N \rightarrow +\infty} \frac{1}{N} \ln [\mathcal{L}(t)]$, which is therefore referred to as the dynamical free energy density⁵¹. Here N denotes the system size. It's worth noticing that there is another definition of the DQPT, which examines the asymptotic late-time steady state of the order parameter^{52–56}. Two types of DQPTs have been discovered that are related in the long-range quantum Ising chain²⁵.

Thus far, many theoretical works have been limited to two-band models, where the periodically spaced critical times are a distinctive feature of DQPTs^{10,50,57}. However, recent studies have extended the theory of DQPT beyond two-band models and provided clear numerical evidence that the critical times of DQPTs may not be uniformly spaced in systems with multiple bands ($l \geq 3$)^{14,31,58}. It's worth noting that non-uniformly spaced critical times have also been observed in non-integrable models⁵¹, quantum spin chains with long-range interactions^{18,19}, and the quantum system with quasiperiodic potential³⁵. However, the reasons for these observations have not been thoroughly explored, and the general properties of DQPTs beyond two-band models have not been conclusively established.

In this paper, we explore DQPTs in the multiband Bloch Hamiltonian, which describes particles in a one-dimensional lattice subjected to the periodic modulation. For instance, the Bloch Hamiltonian in period-two case has four bands ($l = 4$), and that in period-three case has six bands ($l = 6$). We study the scenario of quantum quenches from one of the Bloch states of the pre-quench Hamiltonian. Our findings show that only the type of Bloch state that collapses the band gap at the critical

point induces the occurrence of DQPTs after the quench across the critical point. The condition for the occurrence of DQPTs is confirmed by the proposed criterion in Ref. 14. Similar to studies in Refs. 31 and 58, we observe the critical times in our model are not periodically spaced in the time plane. In other words, the following critical times are not integer multiple of the first critical time t_0^* . Through an analysis of the critical momenta obtained by using the Pancharatnam geometric phase (PGP), we confirm numerically that the first critical momentum, k_c , accompanied by the critical time t_0^* , is determined by the intersections of the overlaps between the initial Bloch states and two Bloch states of the post-quench Hamiltonian which collapse the band gap at the critical point. Interestingly, the critical momenta $k_n, n > 0$ exhibit derivations from the first critical momentum k_c . An intuitive interpretation of behaviors of the DQPT is that quenching from the Bloch state which collapses the band gap at the critical point is similar to that in the two-band systems, and the non-uniformly spaced critical times are induced by the effects of other bands in the multi-band Hamiltonian.

The paper is organized as follows: In Section. II, we introduce the multi-band Bloch Hamiltonian under the periodic effects, and give the band structure of two Bloch Hamiltonian in period-two and period-three cases respectively. Then, the scheme of global quantum quench in the Bloch Hamiltonian is described in Section. III. In Sections. IV and V, we discuss the behaviors of the DQPTs under sudden quenches in the Bloch Hamiltonian $H_k^{l=4}(h)$ and $H_k^{l=6}(h)$ respectively. We summarize our results in Section. VI and discuss the difference of the multiple band systems from the two band models.

II. THE MODELS

We consider the multi-band Bloch Hamiltonian that describes particles in a one-dimensional lattice subjecting to the influence of the periodic modulation with particle-hole symmetry⁵⁹. Assuming a unit lattice constant, the first Brillouin zone is the circle resulting from the interval $[-\pi, \pi]$. The Bloch Hamiltonian is of the form (see Appendix. A)

$$H_k^l(h, \alpha), \quad (2)$$

where l denotes the number of Bloch band, h is the external field, and α represents the strength of periodic modulation, respectively. For instance, the Bloch Hamiltonian in period-two case has $l = 4$ Bloch bands, and that in period-three case has $l = 6$ Bloch bands.

The significant features of quantum phase transitions (QPTs) in associated inhomogeneous quantum systems has been well studied since the mid-20th century. For systems with inhomogeneous interactions, the critical parameters of the QPT satisfy the equation $\prod_{n=1}^N J_n = h^N$, as shown in previous work⁶⁰. Therefore, it is known that the period-two Hamiltonian undergoes the QPT at the

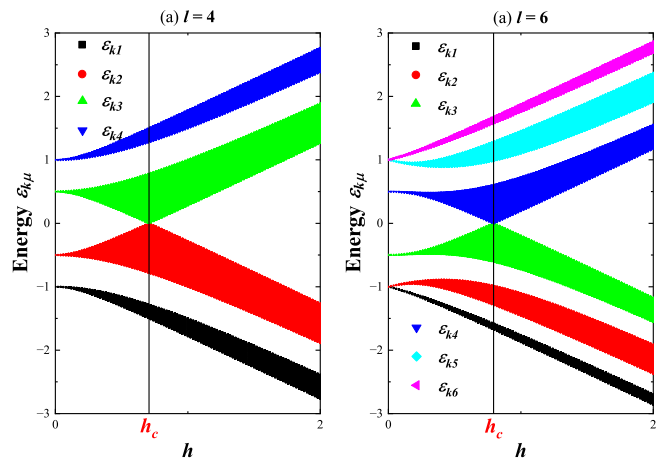


FIG. 1. The energy spectrum of the Bloch Hamiltonian based on the periodic Kitaev model for fixed $\alpha = 0.5$. The resulting energy spectra are shown in (a) for $H_k^{l=4}(h)$, and (b) for $H_k^{l=6}(h)$. In the thermodynamic limit, the energy gap closes at the critical point. For $H_k^{l=4}(h)$, $h_c = \sqrt{\alpha} \approx 0.7071$, and for $H_k^{l=6}(h)$, $h_c = \sqrt[3]{\alpha} \approx 0.7937$.

critical point $h_c = \sqrt{\alpha}$, and the period-three at $h_c = \sqrt[3]{\alpha}$. The QPT reflected in the Bloch Hamiltonian results in the energy gap closing at the critical point in the thermodynamic limit. The energy spectra of the Bloch Hamiltonian $H_k^{l=4}(h)$ and $H_k^{l=6}(h)$ have been plotted in Fig. 1 (a) and (b) respectively, for fixed $\alpha = 0.5$. As shown, the Bloch Hamiltonian $H_k^{l=4}(h)$ displays four bulk states, with a collapse of the energy gap of the middle two occurring at the critical point $h_c = \sqrt{\alpha} \approx 0.7071$. Likewise, the Bloch Hamiltonian $H_k^{l=6}(h)$ features six bulk states, with a collapse of the energy gap of the middle two occurring at the critical point $h_c = \sqrt[3]{\alpha} \approx 0.7937$. It should be noted that the middle two Bloch states, which exhibit a collapse of the energy gap at the critical point under certain parameters, will play a crucial role in inducing the DQPT after a quench across the critical point.

III. SUDDEN QUENCH IN THE BLOCH HAMILTONIAN

In this section, we outline the method for studying the DQPT in the Bloch Hamiltonian by quenching the external field h . In a quantum quench protocol with fixed α , the system's initial state is prepared in one of the Bloch states $|u_{k\mu}^i\rangle$ ($\mu = 1, \dots, l$) of the pre-quench Bloch Hamiltonian $H_k^l(h_0)$. Subsequently, the external field is suddenly switched to another h_1 , which corresponds to the post-quench Bloch Hamiltonian $H_k^l(h_1)$.

To calculate the Loschmidt amplitude according to Eq. (1), we can rewrite the initial state by the superposition of the Bloch state of the post-quench Bloch Hamil-

tonian, which yields

$$|u_{k\mu}^i\rangle = \sum_{\nu=1}^l p_{k\nu} |u_{k\nu}^f\rangle, \quad (3)$$

where $|u_{k\nu}^f\rangle$ ($\nu = 1, \dots, l$) are the Bloch states of the post-quench Hamiltonian, and the expansion coefficients satisfy $p_{k\nu} = \langle u_{k\nu}^f | u_{k\mu}^i \rangle$. Clearly, $|p_{k,\nu=\mu}|^2$ denotes the adiabatic transition probability and $|p_{k,\nu \neq \mu}|^2$ denote the nonadiabatic transition probabilities. The completeness requires $\sum_{\nu=1}^l |p_{k\nu}|^2 = 1$. Then, we obtain the time-evolved state after a quench by

$$|\psi_k(t)\rangle = e^{-iH_k^l(h_1)t} |u_{k\mu}^i\rangle = \sum_{\nu=1}^l e^{-i\varepsilon_{k\nu}^f t} p_{k\nu} |u_{k\nu}^f\rangle, \quad (4)$$

where $\varepsilon_{k\nu}^f$ ($\nu = 1, \dots, l$), subject to

$$H_k^l(h_1) |u_{k\nu}^f\rangle = \varepsilon_{k\nu}^f |u_{k\nu}^f\rangle, \quad (5)$$

are the eigenvalues of the post-quench Bloch Hamiltonian.

Substituting Eq. (4) into Eq. (1), we obtain the Loschmidt amplitude $\mathcal{G}(t) = \prod_{k>0} \mathcal{G}_k(t)$ with

$$\mathcal{G}_k(t) = \sum_{\nu=1}^l |p_{k\nu}|^2 e^{-i\varepsilon_{k\nu}^f t} \quad (6)$$

under the sudden quench from a Bloch state. To obtain the geometric phase during the quench dynamics, it is convenient to express the Loschmidt amplitude in the polar coordinate, which yields

$$\mathcal{G}_k(t) = r_k(t) e^{i\phi_k(t)}, \quad (7)$$

where the phase $\phi_k(t) = \phi_k^{dyn}(t) + \phi_k^G(t)$ consists of two parts: the dynamical phase $\phi_k^{dyn}(t)$ and the PGP $\phi_k^G(t)$. Therefore, the Loschmidt echo $\mathcal{L}(t) = \prod_{k>0} \mathcal{L}_k(t)$ is defined as the modulus of the Loschmidt amplitude

$$\mathcal{L}_k(t) = r_k^2(t). \quad (8)$$

In the thermodynamic limit, the DQPT can be identified by the cusp-like singularity of the dynamical free energy density, which is defined as the rate function of the Loschmidt echo

$$\lambda(t) = - \lim_{N \rightarrow \infty} \frac{1}{N} \ln [\mathcal{L}(t)] = - \int_0^\pi \frac{dk}{2\pi} \ln r_k^2(t). \quad (9)$$

It's important to note that the rate function exhibits the nonanalytic singularity when $r_k(t) = 0$, rendering the phase $\phi_k(t)$ of the Loschmidt amplitude undefined, as per Eq. (7). However, the dynamical phase

$$\phi_k^{dyn}(t) = - \int_0^t ds \langle \psi(s) | H_k^l(h_1) | \psi(s) \rangle = \sum_{\nu=1}^l |p_{k\nu}|^2 \varepsilon_{k\nu}^f t \quad (10)$$

is found to be proportional to time, ensuring that it is always an analytic function of time. Hence, the nonanalytic behavior of the phase $\phi_k(t)$ is manifested in the PGP $\phi_k^G(t)$, which can be extracted from the phase of the Loschmidt amplitude by

$$\phi_k^G(t) = \phi_k(t) - \phi_k^{dyn}(t). \quad (11)$$

The nonanalytic singularity of the Pancharatnam geometric phase is visually demonstrated by the presence of phase vortices in the momentum-time plane^{61–63}.

It is also worth noting that while the Fisher zeros of the Loschmidt amplitude in the complex time plane are effective in illustrating the DQPT in two-band models, they are not applicable in multiple-band systems due to the difficulty in obtaining the solution of

$$\mathcal{G}_{k^*}(t^*) = \sum_{\nu=1}^l |p_{k^*\nu}|^2 e^{-i\varepsilon_{k^*\nu}^f t^*} = 0 \quad (12)$$

for $l > 2$. The best approach to obtain the amplitude condition of the DQPT is through geometric intuition and numerical testing¹⁴. As outlined in the Ref. 14, the criterion for the occurrence of the DQPT can be expressed in a form

$$\psi_{\text{MaxMin}} \equiv \max_{\nu} [\min_k |p_{k\nu}|], \quad (13)$$

$$\psi_{\text{MaxMin}} = 0 \Leftrightarrow \text{DQPT}. \quad (14)$$

In the following, we discuss the numerical results of the dynamical behaviors after a quench in two Bloch Hamiltonian $H_k^{l=4}(h)$ and $H_k^{l=6}(h)$, respectively.

IV. THE BLOCH HAMILTONIAN $H_k^{l=4}(h)$ IN PERIOD-TWO CASE

In this section, we focus on the dynamical behavior after a quench in the period-two Bloch Hamiltonian $H_k^{l=4}(h)$. For the purpose of comparison, we begin by examining the rate functions of the Loschmidt echo in quenches from the Bloch states $|u_{k1}^i\rangle$ and $|u_{k2}^i\rangle$, respectively. Note that the situations of quenching from $|u_{k3}^i\rangle$ and $|u_{k4}^i\rangle$ are similar to that from $|u_{k2}^i\rangle$ and $|u_{k1}^i\rangle$, respectively, due to the symmetric energy spectra of the Bloch Hamiltonian around zero energy, i.e., $\varepsilon_{k1} = -\varepsilon_{k4}$ and $\varepsilon_{k2} = -\varepsilon_{k3}$, as depicted in Fig. 1 (a), which can also be attributed to the particle-hole symmetry⁵⁹. Therefore, it is sufficient to discuss the cases of quench from the Bloch states $|u_{k1}^i\rangle$ and $|u_{k2}^i\rangle$ only.

Fig. 2 illustrates the rate functions of the Loschmidt echo in three quenching scenarios from the lowest Bloch state $|u_{k1}^i\rangle$ of the pre-quench Hamiltonian, where the quenches in (a) and (b) do not cross the critical point $h_c \approx 0.7071$, while those in (c) and (d) do. Notably, the rate functions display smooth crossovers in both cases,

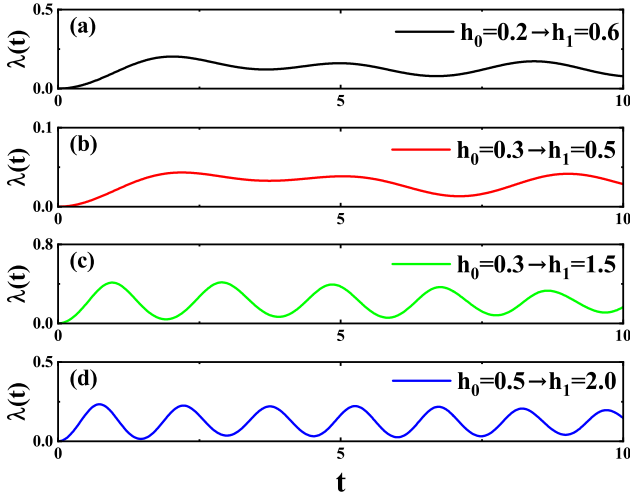


FIG. 2. The rate functions associated with the Bloch Hamiltonian $H_k^{l=4}(h)$ after quenches from the lowest Bloch states $|u_{k1}^i\rangle$, where the quenches in (a) and (b) do not cross the critical point $h_c \approx 0.7071$, while those in (c) and (d) do. As depicted, the rate functions exhibit smooth crossovers in these cases, suggesting the absence of DQPTs.

suggesting that a DQPT is unlikely to occur in quenches from the lowest Bloch states.

Similarly, we present the rate functions of the Loschmidt echo for three instances of quenches from the second lowest Bloch state $|u_{k2}^i\rangle$ of the pre-quench Hamiltonian in Fig. 3. Notably the quenches in (a) and (b) do not cross the critical point $h_c \approx 0.7071$, while those in (c) and (d) do. Clearly, the rate functions exhibit a smooth behavior with respect to time when the quenches do not cross the critical point h_c , suggesting the absence of DQPT. Conversely, for quenches that cross h_c , the rate functions exhibit cusp-like singularities at the critical times t_n^* . Thus, the occurrence of DQPT depends on whether the quench crosses the critical point in the case from the Bloch state $|u_{k2}^i\rangle$, similar to the DQPT behavior observed in the quantum Ising chain⁴⁸.

Another intriguing observation worth noting is that the critical times of the DQPT are not spaced uniformly. In Fig. 3 (c) and (d), we discovered that when dividing the time axis by the first critical time t_0^* , the critical times t_n^* are not integer multiple of t_0^* . This finding suggests that the critical times in the multi-band Hamiltonian are no longer periodically spaced as they are in the two-band model.

While the non-uniformly spaced critical times of the DQPT have previously been observed in both the disordered periodic Kitaev chain⁵⁸ and the extended XY chain under the influence of an alternating external field³¹, the underlying reason for this phenomenon has yet to be fully elucidated. Here we try to explain the reason via the critical momentums corresponding to the critical times. Since it is difficult to obtain the critical momentums directly from the Loschmidt amplitude or the Loschmidt

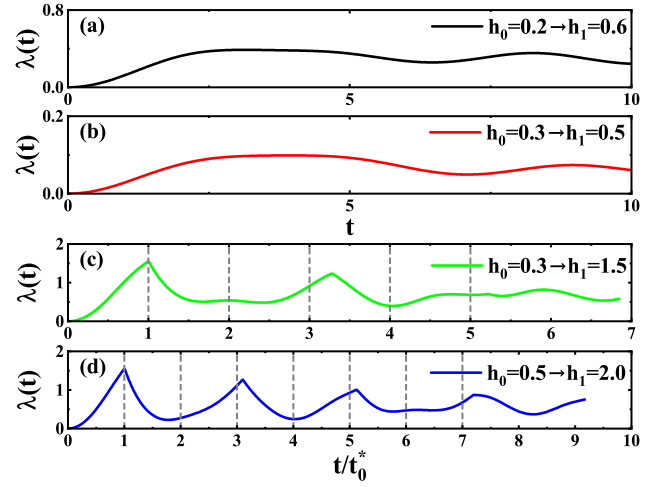


FIG. 3. The rate functions associated with the Bloch Hamiltonian $H_k^{l=4}(h)$ after quenches from the second lowest Bloch states $|u_{k2}^i\rangle$. Similarly the quenches in (a) and (b) do not cross the critical point $h_c \approx 0.7071$, while those in (c) and (d) do. As depicted, the rate functions exhibit cusp-like singularities at the critical times t_n^* when the quench is across $h_c \approx 0.7071$. Otherwise, the DQPTs are absent. Upon scaling the time axis by the first critical time t_0^* , we observe that the critical times t_n^* are not integer multiples of t_0^* . This non-uniform spacing of critical times differs from that observed in two-band models

echo, we instead use the property that the PGP shows non-analytic vortices at critical momentums.

In Fig. 4, we show a contour plot of the PGP $\phi_k^G(t)$ in the (k, t) plane, with the quench path ranging from $h_0 = 0.3$ to $h_1 = 1.5$. Unlike the cases observed in two-band models or the periodic quantum Ising chain under the quench from the ground states of the pre-quench Hamiltonian⁶⁴, the critical momentums associated with the critical times t_n^* ($n > 0$) exhibit derivation from the critical momentum k_c , which corresponds to the first critical time t_0^* . Furthermore, by extensive numerical simulations, we find that the critical momentum k_c associated with the first critical time t_0^* actually satisfies $|p_{k_c 2}|^2 = |p_{k_c 3}|^2$, i.e.,

$$|\langle u_{k_c 2}^f | u_{k_c 2}^i \rangle|^2 = |\langle u_{k_c 3}^f | u_{k_c 2}^i \rangle|^2 < \frac{1}{2}. \quad (15)$$

Fig. 5 plots the expansion coefficients $|p_{k\nu}|^2 = |\langle u_{k\nu}^f | u_{k\nu}^i \rangle|^2$ as a function of k in the quench path from $h_0 = 0.3$ to $h_1 = 1.5$. As depicted, the coefficients $|p_{k2}|^2$ and $|p_{k3}|^2$ have an intersection at the critical time k_c . The origin of k_c provides us valuable insight of the multi-band systems, similar to the two-band models, where the critical momentum typically arises from the expansion coefficients $p_k = 1 - p_k = \frac{1}{2}$ in such models^{57,61,65,66}. When considering the quench from the Bloch state $|u_{k2}^i\rangle$, the situation is analogous to that of two-band models, with the only distinction being the presence of additional terms $|p_{k1}|^2$ and $|p_{k4}|^2$, resulting in $|p_{k2}|^2 = |p_{k3}|^2 < \frac{1}{2}$

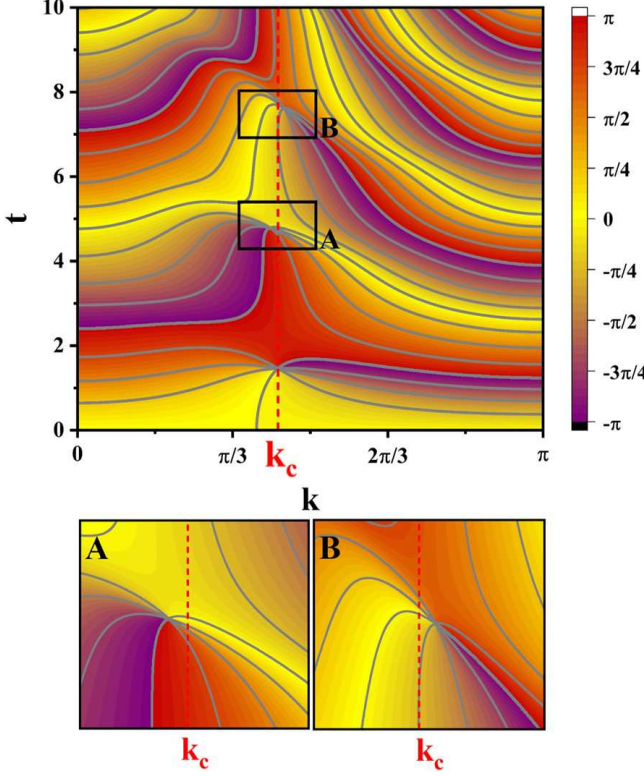


FIG. 4. The contour plot of the PGP $\phi_k^G(t)$ is shown as a function of (k, t) for the quench across the critical point h_c and from the Bloch state $|u_{k2}^i\rangle$. The quench path is from $h_0 = 0.3$ to $h_1 = 1.5$. The labeled critical momentum k_c corresponds to the first critical time t_0^* . Graphs A and B are enlarged figures that highlight the critical momenta corresponding to the critical times t_1^* and t_2^* , respectively.

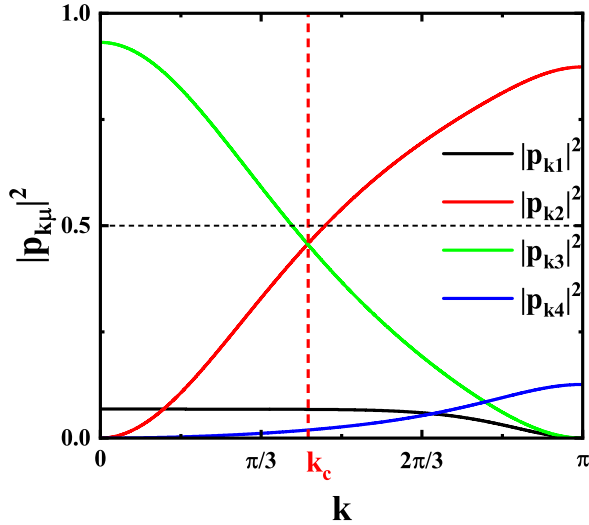


FIG. 5. The expansion coefficients $|p_{k\nu}|^2 = |\langle u_{k\nu}^f | u_{k\mu}^i \rangle|^2$ in the quench from the Bloch state $|u_{k2}^i\rangle$. The quench path is from $h_0 = 0.3$ to $h_1 = 1.5$.

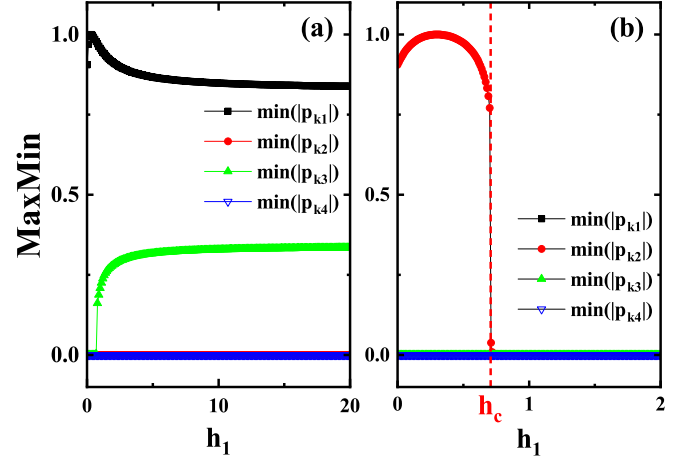


FIG. 6. Plot of $\psi_{\text{MaxMin}}(h_1)$ [Eqs. (13) and (14)] as functions of the post-quench parameter h_1 in the Bloch Hamiltonian $H_k^{l=4}(h)$. The initial state is prepared in one of the two Bloch bands $|u_{k1}^i\rangle$ for (a) and $|u_{k2}^i\rangle$ for (b) with the pre-quench parameter $h_0 = 0.3$, respectively. In each case, there are four components $\min(|p_{k\nu}|)$ $\nu = 1, \dots, 4$. The occurrence of DQPT can be identified by $\psi_{\text{MaxMin}}(h_1) = \text{Max}[\min(|p_{k\nu}|)] = 0$.

at the critical momenta k_c . The derivation of the critical momenta k_{cn} ($n > 0$) from the first critical momentum k_c can be explained via the geometrical interpolation. According to Eq. (12), the occurrence of the DQPT $\mathcal{G}(t^*) = 0$ can be understood geometrically as the complex numbers $z_\nu = |p_{k\nu}^*|^2 e^{-i\varepsilon_{k\nu}^f t^*}$ ($\nu = 1, \dots, 4$) forming a closed polygon in the complex plane at t^* ^{14,65}. Our analysis begins at the first critical time t_0^* , where the complex numbers z_ν form a closed polygon. Subsequently, all z_ν can be viewed as rotating in the complex plane with the angular velocity $\varepsilon_{k\nu}^f$ (notably, $\varepsilon_{k1}^f = -\varepsilon_{k4}^f$ and $\varepsilon_{k2}^f = -\varepsilon_{k3}^f$). At the subsequent critical times, A mismatch will arise in the complex numbers z_ν due to the discrepancy between $\varepsilon_{k\nu}^f$, specifically, $\varepsilon_{k1}^f \neq \varepsilon_{k2}^f$ and $\varepsilon_{k3}^f \neq \varepsilon_{k4}^f$. Consequently, the complex numbers form the closed polygon at another critical momentum that deviates from k_c .

To conclude this section, we verify the condition for the DQPT to occur in the Bloch Hamiltonian $H_k^{l=4}(h)$ by Eqs. (13) and (14). Fig. 6 displays the $\psi_{\text{MaxMin}}(h_1)$ as functions of the post-quench parameter h_1 in the quenches from the Bloch bands $|u_{k1}^i\rangle$ and $|u_{k2}^i\rangle$ with the pre-quench parameter $h_0 = 0.3$, respectively. As observed in Fig. 6 (a), the $\psi_{\text{MaxMin}}(h_1)$ is equal to $\text{Min}(|p_{k1}|)$, which is always larger than zero. This can be explained by the fact that owing to the gap between ε_{k1}^f and the other bands, the system will be positioned at the instantaneous lowest state $|u_{k1}^f\rangle$, corresponding to the adiabatic evolution. However, things are different when the quench is from the state $|u_{k2}^i\rangle$, at which the energy gap between ε_{k2} and ε_{k3} vanishes at the critical point h_c . Consequently, we observe that $\psi_{\text{MaxMin}}(h_1)$ changes

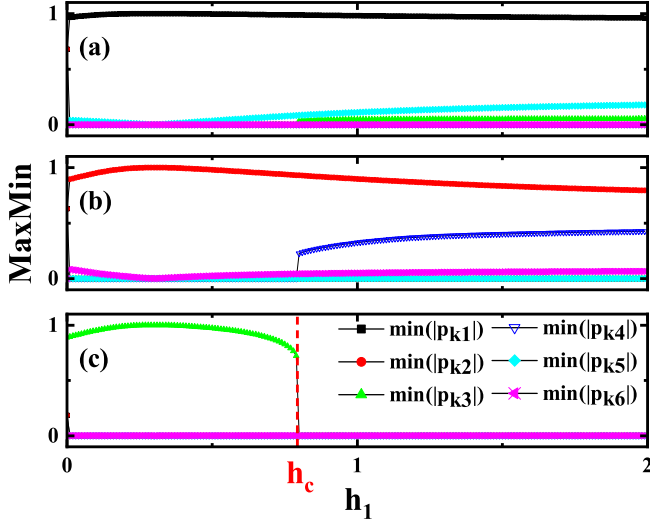


FIG. 7. Plot of $\psi_{\text{MaxMin}}(h_1)$ [Eqs. (13) and (14)] as functions of the post-quench parameter h_1 in the Bloch Hamiltonian $H_k^{l=6}(h)$. The initial state is prepared in one of the three Bloch bands $|u_{k1}^i\rangle$ for (a), $|u_{k2}^i\rangle$ for (b) and $|u_{k3}^i\rangle$ for (c) with the pre-quench parameter $h_0 = 0.3$, respectively. In each case, there are six components $\min(|p_{k\nu}|)$ $\nu = 1, \dots, 6$. The occurrence of DQPT can be identified by $\psi_{\text{MaxMin}}(h_1) = \text{Max}[\min(|p_{k\nu}|)] = 0$.

from nonzero to zero at the critical point $h_1 = h_c$ [refer to Fig. 6 (b)]. Evidently, the outcomes presented in Fig. 6 are consistent with the conclusions we inferred earlier, i.e., the occurrence of DQPT in the Bloch Hamiltonian $H_k^{l=4}(h)$ requires the quench from the Bloch state $|u_{k2}^i\rangle$ and across the critical point h_c .

V. THE BLOCH HAMILTONIAN $H_k^{l=6}(h)$ IN PERIOD-THREE CASE

In this section, we continue to delve into the behavior of DQPT in the Bloch Hamiltonian $H_k^{l=6}(h)$. Based on the findings in Section. III, it is evident that the outcomes presented by ψ_{MaxMin} are consistent with those inferred from the rate functions or the PGP. Moreover, the ψ_{MaxMin} provides a more intuitive depiction of the conditions under which the DQPT occurs. Therefore, we commence with a discussion of the ψ_{MaxMin} in this section.

In Fig. 7, we plot the $\psi_{\text{MaxMin}}(h_1)$ as functions of the post-quench parameter h_1 in the quenches from the Bloch bands $|u_{k1}^i\rangle$, $|u_{k2}^i\rangle$ and $|u_{k3}^i\rangle$ with the pre-quench parameter $h_0 = 0.3$, respectively. As depicted in Fig. 7 (a) and (b), the $\psi_{\text{MaxMin}}(h_1)$ are actually equal to $\text{Min}(|p_{k1}|)$ and $\text{Min}(|p_{k2}|)$ respectively, when the quench is from the Bloch bands $|u_{k1}^i\rangle$ and $|u_{k2}^i\rangle$. However, upon quenching from the Bloch state $|u_{k3}^i\rangle$, we observe that the $\psi_{\text{MaxMin}}(h_1)$ changes from a nonzero value to zero at the critical point $h_1 = h_c \approx 0.7937$ [refer to Fig. 7 (c)]. Hence, similar to the case in the Bloch Hamiltonian

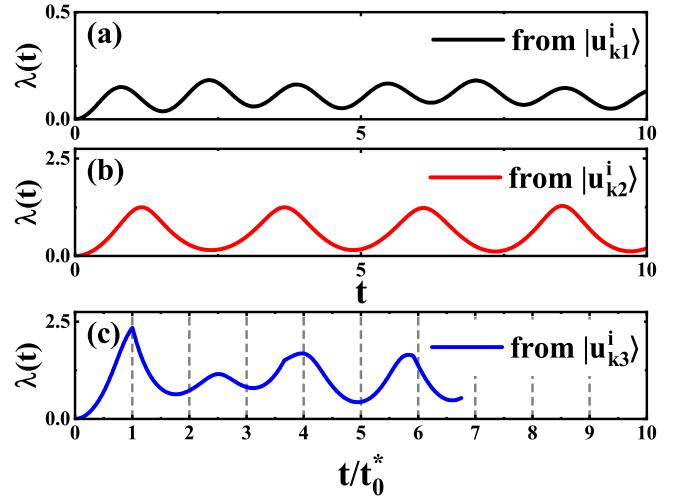


FIG. 8. The rate functions in the Bloch Hamiltonian $H_k^{l=6}(h)$ after quenches from the Bloch bands $|u_{k1}^i\rangle$ for (a), $|u_{k2}^i\rangle$ for (b) and $|u_{k3}^i\rangle$ for (c), respectively. The quench path is from $h_0 = 0.3$ to $h_1 = 1.5$, which crosses the critical point $h_c \approx 0.7937$. In (c), the time axis are scaled by the first critical time t_0^* to show that the critical times are not spaced uniformly.

$H_k^{l=4}(h)$, the DQPT only occurs in the quench from the Bloch state $|u_{k3}^i\rangle$ and across the critical point h_c . Here the Bloch state $|u_{k3}^i\rangle$ is akin to the Bloch state $|u_{k2}^i\rangle$ of the Bloch Hamiltonian $H_k^{l=4}(h)$, whose energy band collapses the gap at the critical point h_c .

To explicitly corroborate the results inferred from the $\psi_{\text{MaxMin}}(h_1)$, we provide a typical example of a quench path. Fig. 8 displays the rate functions in the Bloch Hamiltonian $H_k^{l=4}(h)$ for quenches from the Bloch bands $|u_{k1}^i\rangle$ for (a), $|u_{k2}^i\rangle$ for (b) and $|u_{k3}^i\rangle$ for (c), respectively. The quench path is from $h_0 = 0.3$ to $h_1 = 1.5$. As depicted in Fig. 8 (a) and (b), where the quenches are from the Bloch bands $|u_{k1}^i\rangle$ and $|u_{k2}^i\rangle$ respectively, the rate functions are smooth functions of time, indicating the absence of DQPT in these cases of quenches. However, upon quenching from the Bloch band $|u_{k3}^i\rangle$ [refer to Fig. 8 (c)], the rate function displays cusp-like singularities at the critical times, and the critical times are not spaced periodically either.

Likewise, the DQPT in the Bloch Hamiltonian $H_k^{l=6}(h)$ exhibits the same behavior as that in the Bloch Hamiltonian $H_k^{l=4}(h)$. By analyzing the reason of the non-uniformly spaced critical times, we present the contour plot of the PGP $\phi_k^G(t)$ as a function of (k, t) for the quench across the critical point h_c and from the Bloch state $|u_{k3}^i\rangle$ in Fig. 9. The quench path is from $h_0 = 0.3$ to $h_1 = 1.5$. Just like in the Bloch Hamiltonian $H_k^{l=4}(h)$, we observe that, in the Bloch Hamiltonian $H_k^{l=6}(h)$, the critical momentums associated with the critical times t_n^* ($n > 0$) deviates from the critical momentum k_c marked in Fig. 9, corresponding to the first critical time t_0^* . The deviation of the critical momentum can also be explained in the same way as we have already elucidated in the

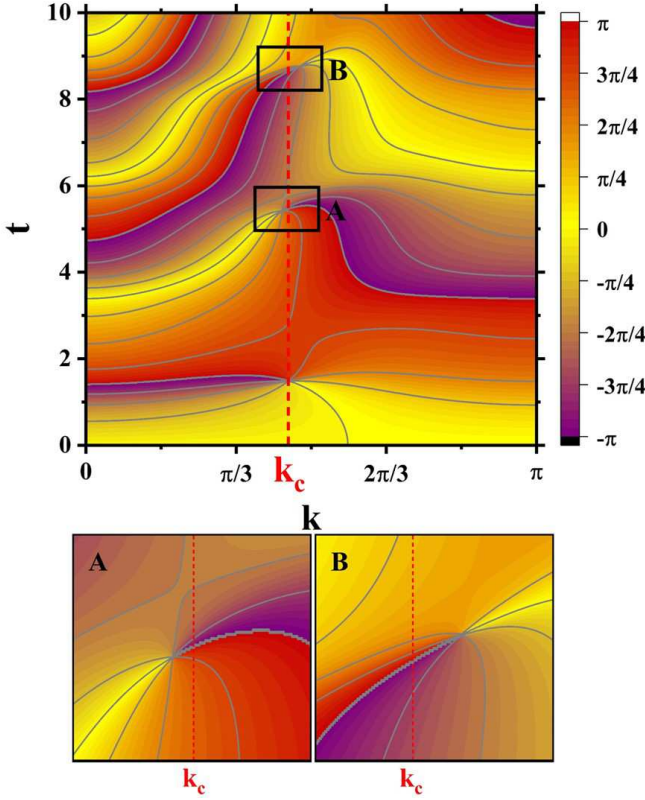


FIG. 9. The contour plot of the PGP $\phi_k^G(t)$ as a function of (k, t) for the quench across the critical point h_c and from the Bloch state $|u_{k3}^i\rangle$. The quench path is from $h_0 = 0.3$ to $h_1 = 1.5$. The labeled critical momentum k_c corresponds to the first critical time t_0^* . Graphs A and B are enlarged figures that highlight the critical momenta corresponding to the critical times t_1^* and t_2^* , respectively.

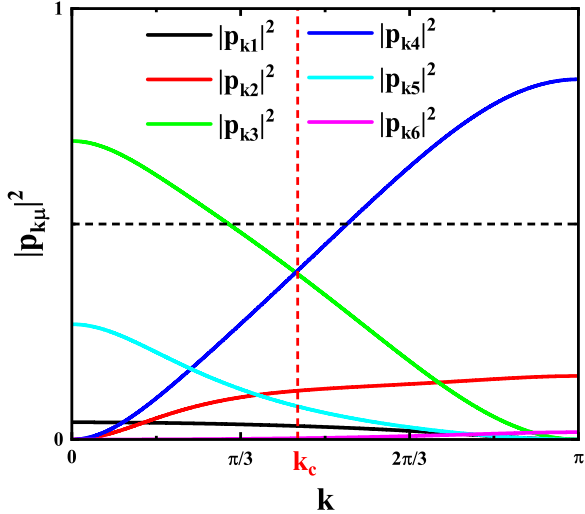


FIG. 10. The expansion coefficients $|p_{k\nu}|^2 = |\langle u_{k\nu}^f | u_{k\mu}^i \rangle|^2$, $\nu = 1, 2, 3$ in the quench from the Bloch state $|u_{k3}^i\rangle$. The quench path is from $h_0 = 0.3$ to $h_1 = 1.5$.

Bloch Hamiltonian $H_k^{l=4}(h)$. In Fig. 10, we show the expansion coefficients $|p_{k\nu}|^2 = |\langle u_{k\nu}^f | u_{k\mu}^i \rangle|^2$, $\nu = 1, 2, 3$ in the quench from the Bloch state $|u_{k3}^i\rangle$. It is apparent that the critical momentum k_c is actually determined by

$$|\langle u_{k_c3}^f | u_{k_c3}^i \rangle|^2 = |\langle u_{k_c4}^f | u_{k_c3}^i \rangle|^2 < \frac{1}{2}. \quad (16)$$

It should be noted that the Eq. (16) has undergone extensive numerical testing. The reason for the values $|p_{k3}|^2 = |p_{k4}|^2$ being smaller than $\frac{1}{2}$ is due to the presence of additional terms $|p_{k1}|^2$, $|p_{k2}|^2$, $|p_{k5}|^2$ and $|p_{k6}|^2$. The relation (16) will be broken at later critical times t_n^* ($n > 0$) due to the mismatch induced by the effect of multiple bands, as discussed in the case of the Bloch Hamiltonian $H_k^{l=4}$. Consequently, the critical momentum will deviate from the first critical momentum k_c , resulting in non-uniformly spaced critical times of DQPTs in the multi-band models.

VI. CONCLUSION

In this paper, we investigate the DQPT in the Bloch Hamiltonian with multiple Bloch bands after a quench from one of the Bloch bands. Our study reveals that the occurrence of the DQPT is highly dependent on the initial states, where the non-adiabatic evolution caused by collapsing the band gap plays a crucial role. DQPT is only present when the quench is from a particular type of Bloch state, whose energy band collapses the band gap at the critical point h_c and crosses the critical point. This can be understood by that the quench from this type of Bloch state, which collapses the band gap at h_c , is more like the case in the two bands models. The more obvious sign is that the critical momentum k_c corresponding to the first critical time t_0^* satisfies $|p_{k_c, \nu^*}|^2 = |p_{k_c, \nu^*+1}|^2 < \frac{1}{2}$, which is quite similar to the condition $p_{k_c} = 1 - p_{k_c} = \frac{1}{2}$ in two bands models^{57,61,65,66}. However, there are additional terms $|p_{k\nu}|^2$, $\nu \neq \nu^*$, in the multiple band, which results in the value of above equation is smaller than $\frac{1}{2}$. Furthermore, according to the geometrical interpretation, the non-periodically spaced critical times arise due to the complex number z_ν mismatch caused by the the energy band differences, where the energies $\varepsilon_{k\nu}^f$ in fact represent the angular velocities. Consequently, the critical momentum k_{cn} ($n > 0$) corresponding to the later critical times t_n^* deviate from the first critical momentum k_c . Our findings contribute to a better understanding of the characteristics of non-equilibrium systems surrounding DQPTs.

ACKNOWLEDGMENTS

The work is supported by National Key Basic Research Program of China (No. 2020YFB0204800), National Natural Science Foundation of China (No. 12074064),

and Key Research Projects of Zhejiang Lab (Nos. 2021PB0AC01 and 2021PB0AC02).

Appendix A: Bloch Hamiltonian based on the periodic Kitaev model

We study the Hamiltonian that describes particles in a one-dimensional lattice subjecting to periodic effects, based on the one-dimensional Kitaev model

$$H = -\frac{1}{2} \sum_{n=1}^N \{ [J_n c_n^\dagger c_{n+1} + \Delta_n c_n^\dagger c_{n+1}^\dagger + h c_n^\dagger c_n] + h.c. \}, \quad (\text{A1})$$

where J_n are hopping interactions, Δ_n are superconducting gaps, and h is the external field. For simplicity, we take $\Delta_n = J_n$ in our work.

Under the periodic boundary condition, we can express the Hamiltonian of the system as the form

$$H = \sum_{k>0} \Psi_k^\dagger H_k \Psi_k \quad (\text{A2})$$

in the momentum space $k > 0$, where the spinor operator is $\Psi_k^\dagger = (c_{k1}^\dagger, c_{-k1}, \dots, c_{kL}^\dagger, c_{-kL})$ and H_k is the associated Bloch Hamiltonian.

Specifically, for the period-two case, we consider the nearest-neighbor interactions:

$$J_n = \begin{cases} J_1, & \text{odd } n, \\ J_2, & \text{even } n. \end{cases} \quad (\text{A3})$$

Here, we set $\alpha = J_2/J_1$ and $J_1 = J = 1$ without losing generality, so that α denotes the strength of the periodic modulation. Apparently, $\alpha = 0.5$ denotes the strongest periodic modulation, and $\alpha = 1$ recovers the homogeneous case. The Bloch Hamiltonian of the period-two case is a 4×4 Hermitian matrix yielding

$$H_k^{l=4}(h, \alpha) = \frac{J}{2} \begin{pmatrix} -2h/J & 0 & -(1 + \alpha e^{-ik}) & -(1 - \alpha e^{-ik}) \\ 0 & 2h/J & (1 - \alpha e^{-ik}) & (1 + \alpha e^{-ik}) \\ -(1 + \alpha e^{ik}) & (1 - \alpha e^{ik}) & -2h/J & 0 \\ -(1 - \alpha e^{ik}) & (1 + \alpha e^{ik}) & 0 & 2h/J \end{pmatrix}, \quad (\text{A4})$$

where $l = 4$ denotes that the Bloch Hamiltonian has four Bloch bands.

Similarly, for the period-three case, we consider the nearest-neighbor interactions ($p \in \mathbb{Z}$)

$$J_n = \begin{cases} J, & n = 3p - 2, \\ \alpha J, & n = 3p - 1, \\ \beta J, & n = 3p. \end{cases} \quad (\text{A5})$$

For simplicity, we set $\beta = 1$ and use α to control the strength of the periodic modulation. The Bloch Hamiltonian of the period-three case is a 6×6 Hermitian matrix yielding

$$H_k^{l=6}(h, \alpha) = \frac{J}{2} \begin{pmatrix} -2h/J & 0 & -1 & -1 & -e^{-ik} & e^{-ik} \\ 0 & 2h/J & 1 & 1 & -e^{-ik} & e^{-ik} \\ -1 & 1 & -2h/J & 0 & -\alpha & -\alpha \\ -1 & 1 & 0 & 2h/J & \alpha & \alpha \\ -e^{ik} & -e^{ik} & -\alpha & \alpha & -2h/J & 0 \\ e^{ik} & e^{ik} & -\alpha & \alpha & 0 & 2h/J \end{pmatrix}, \quad (\text{A6})$$

where $l = 6$ denotes that the Bloch Hamiltonian has six

Bloch bands.

* guohao.ph@seu.edu.cn

† ygw@tsinghua.edu.cn

¹ I. Bloch, J. Dalibard, and W. Zwerger, Rev. Mod. Phys. **80**, 885 (2008).

² M. Lewenstein, A. Sanpera, and V. Ahufinger, *Ultracold Atoms in Optical Lattices: Simulating quantum many-body systems* (Oxford University Press, 2012).

³ M. Belsley, Contemporary Physics **54**, 112 (2013).

- ⁴ A. Polkovnikov, K. Sengupta, A. Silva, and M. Vengalattore, *Rev. Mod. Phys.* **83**, 863 (2011).
- ⁵ A. Mitra, *Annual Review of Condensed Matter Physics* **9**, 245 (2018).
- ⁶ W. H. Zurek, U. Dorner, and P. Zoller, *Phys. Rev. Lett.* **95**, 105701 (2005).
- ⁷ F. Andraschko and J. Sirker, *Phys. Rev. B* **89**, 125120 (2014).
- ⁸ M. Heyl, *Phys. Rev. Lett.* **113**, 205701 (2014).
- ⁹ J. M. Hickey, S. Genway, and J. P. Garrahan, *Phys. Rev. B* **89**, 054301 (2014).
- ¹⁰ S. Vajna and B. Dóra, *Phys. Rev. B* **89**, 161105 (2014).
- ¹¹ M. Heyl, *Phys. Rev. Lett.* **115**, 140602 (2015).
- ¹² M. Schmitt and S. Kehrein, *Phys. Rev. B* **92**, 075114 (2015).
- ¹³ S. Vajna and B. Dóra, *Phys. Rev. B* **91**, 155127 (2015).
- ¹⁴ Z. Huang and A. V. Balatsky, *Phys. Rev. Lett.* **117**, 086802 (2016).
- ¹⁵ U. Bhattacharya, S. Bandyopadhyay, and A. Dutta, *Phys. Rev. B* **96**, 180303 (2017).
- ¹⁶ U. Bhattacharya and A. Dutta, *Phys. Rev. B* **96**, 014302 (2017).
- ¹⁷ A. Gómez-León and P. C. E. Stamp, *Phys. Rev. B* **95**, 054402 (2017).
- ¹⁸ J. C. Halimeh and V. Zauner-Stauber, *Phys. Rev. B* **96**, 134427 (2017).
- ¹⁹ I. Homrighausen, N. O. Abeling, V. Zauner-Stauber, and J. C. Halimeh, *Phys. Rev. B* **96**, 104436 (2017).
- ²⁰ S. A. Weidinger, M. Heyl, A. Silva, and M. Knap, *Phys. Rev. B* **96**, 134313 (2017).
- ²¹ C. Yang, Y. Wang, P. Wang, X. Gao, and S. Chen, *Phys. Rev. B* **95**, 184201 (2017).
- ²² A. Kosior and K. Sacha, *Phys. Rev. A* **97**, 053621 (2018).
- ²³ H. Lang, Y. Chen, Q. Hong, and H. Fan, *Phys. Rev. B* **98**, 134310 (2018).
- ²⁴ B. Mera, C. Vlachou, N. Paunković, V. R. Vieira, and O. Viyuela, *Phys. Rev. B* **97**, 094110 (2018).
- ²⁵ B. Žunković, M. Heyl, M. Knap, and A. Silva, *Phys. Rev. Lett.* **120**, 130601 (2018).
- ²⁶ M. Abdi, *Phys. Rev. B* **100**, 184310 (2019).
- ²⁷ Y.-P. Huang, D. Banerjee, and M. Heyl, *Phys. Rev. Lett.* **122**, 250401 (2019).
- ²⁸ A. Lahiri and S. Bera, *Phys. Rev. B* **99**, 174311 (2019).
- ²⁹ T. Liu and H. Guo, *Phys. Rev. B* **99**, 104307 (2019).
- ³⁰ K. Cao, W. Li, M. Zhong, and P. Tong, *Phys. Rev. B* **102**, 014207 (2020).
- ³¹ S. Haldar, S. Roy, T. Chanda, A. Sen(De), and U. Sen, *Phys. Rev. B* **101**, 224304 (2020).
- ³² T. H. Kyaw, V. M. Bastidas, J. Tangpanitanon, G. Romero, and L.-C. Kwek, *Phys. Rev. A* **101**, 012111 (2020).
- ³³ Y. Wu, *Phys. Rev. B* **101**, 064427 (2020).
- ³⁴ J. C. Halimeh, M. Van Damme, L. Guo, J. Lang, and P. Hauke, *Phys. Rev. B* **104**, 115133 (2021).
- ³⁵ R. Modak and D. Rakshit, *Phys. Rev. B* **103**, 224310 (2021).
- ³⁶ K. Cao, M. Zhong, and P. Tong, *Chinese Physics B* **31**, 060505 (2022).
- ³⁷ R. B. Jensen, S. P. Pedersen, and N. T. Zinner, *Phys. Rev. B* **105**, 224309 (2022).
- ³⁸ K. Wrześniewski, I. Weymann, N. Sedlmayr, and T. Domański, *Phys. Rev. B* **105**, 094514 (2022).
- ³⁹ X.-Y. Hou, Q.-C. Gao, H. Guo, and C.-C. Chien, *Phys. Rev. B* **106**, 014301 (2022).
- ⁴⁰ P. Jurcevic, H. Shen, P. Hauke, C. Maier, T. Brydges, C. Hempel, B. P. Lanyon, M. Heyl, R. Blatt, and C. F. Roos, *Phys. Rev. Lett.* **119**, 080501 (2017).
- ⁴¹ J. Zhang, G. Pagano, P. W. Hess, A. Kyprianidis, P. B. Ecker, H. Kaplan, A. V. Gorshkov, Z. X. Gong, and C. Monroe, *Nature* **551**, 601 (2017).
- ⁴² N. Fläschner, D. Vogel, M. Tarnowski, B. S. Rem, D. S. Lühmann, M. Heyl, J. C. Budich, L. Mathey, K. Sengstock, and C. Weitenberg, *Nature Physics* **14**, 265 (2017).
- ⁴³ X.-Y. Guo, C. Yang, Y. Zeng, Y. Peng, H.-K. Li, H. Deng, Y.-R. Jin, S. Chen, D. Zheng, and H. Fan, *Phys. Rev. Applied* **11**, 044080 (2019).
- ⁴⁴ K. Wang, X. Qiu, L. Xiao, X. Zhan, Z. Bian, W. Yi, and P. Xue, *Phys. Rev. Lett.* **122**, 020501 (2019).
- ⁴⁵ Z. Chen, J.-M. Cui, M.-Z. Ai, R. He, Y.-F. Huang, Y.-J. Han, C.-F. Li, and G.-C. Guo, *Phys. Rev. A* **102**, 042222 (2020).
- ⁴⁶ X. Nie, B.-B. Wei, X. Chen, Z. Zhang, X. Zhao, C. Qiu, Y. Tian, Y. Ji, T. Xin, D. Lu, and J. Li, *Phys. Rev. Lett.* **124**, 250601 (2020).
- ⁴⁷ T. Tian, H.-X. Yang, L.-Y. Qiu, H.-Y. Liang, Y.-B. Yang, Y. Xu, and L.-M. Duan, *Phys. Rev. Lett.* **124**, 043001 (2020).
- ⁴⁸ M. Heyl, A. Polkovnikov, and S. Kehrein, *Phys. Rev. Lett.* **110**, 135704 (2013).
- ⁴⁹ A. A. Zvyagin, *Low Temperature Physics* **42**, 971 (2016).
- ⁵⁰ M. Heyl, *Reports on Progress in Physics* **81**, 054001 (2018).
- ⁵¹ C. Karrasch and D. Schuricht, *Phys. Rev. B* **87**, 195104 (2013).
- ⁵² E. A. Yuzbashyan, O. Tsyplatyev, and B. L. Altshuler, *Phys. Rev. Lett.* **96**, 097005 (2006).
- ⁵³ P. Barmettler, M. Punk, V. Gritsev, E. Demler, and E. Altman, *Phys. Rev. Lett.* **102**, 130603 (2009).
- ⁵⁴ M. Eckstein, M. Kollar, and P. Werner, *Phys. Rev. Lett.* **103**, 056403 (2009).
- ⁵⁵ B. Sciolla and G. Birolì, *Phys. Rev. Lett.* **105**, 220401 (2010).
- ⁵⁶ J. Dziarmaga, *Advances in Physics* **59**, 1063 (2010).
- ⁵⁷ S. Sharma, S. Suzuki, and A. Dutta, *Phys. Rev. B* **92**, 104306 (2015).
- ⁵⁸ C. B. Mendl and J. C. Budich, *Phys. Rev. B* **100**, 224307 (2019).
- ⁵⁹ A. Altland and M. R. Zirnbauer, *Phys. Rev. B* **55**, 1142 (1997).
- ⁶⁰ P. Pfeuty, *Phys. Lett. A* **72**, 245 (1979).
- ⁶¹ S. Sharma, U. Divakaran, A. Polkovnikov, and A. Dutta, *Phys. Rev. B* **93**, 144306 (2016).
- ⁶² A. Dutta and A. Dutta, *Phys. Rev. B* **96**, 125113 (2017).
- ⁶³ K. Cao, S. Yang, Y. Hu, and G. Yang, *arXiv: 2211.15976* 10.48550/arXiv.2211.15976.
- ⁶⁴ K. Cao, M. Zhong, and P. Tong, *J. Phys. A-Math. Theor.* **55**, 365001 (2022).
- ⁶⁵ J. M. Zhang and H.-T. Yang, *Europhysics Letters* **114**, 60001 (2016).
- ⁶⁶ U. Divakaran, S. Sharma, and A. Dutta, *Phys. Rev. E* **93**, 052133 (2016).